NIH Public Access
Author Manuscript
Neuroimage. Author manuscript; available in PMC 2011 June 1.

Published in final edited form as:
Neuroimage. 2010 June ; 51(2): 616–622. doi:10.1016/j.neuroimage.2010.02.050.

MR Imaging of High-Grade Brain Tumors Using Endogenous Protein and Peptide-Based Contrast

Zhibo Wen[a,b,*], **Shuguang Hu**[c], **Fanheng Huang**[a], **Xianlong Wang**[a], **Linglang Guo**[d], **Xianyue Quan**[a], **Silun Wang**[b], and **Jinyuan Zhou**[b,e,*]

[a]Department of Radiology, Zhujiang Hospital, Southern Medical University, Guangzhou, Guangdong, China

[b]Division of MR Research, Department of Radiology, Johns Hopkins University, MD, United States

[c]Philips Healthcare, Guangzhou, Guangdong, China

[d]Department of Pathology, Zhujiang Hospital, Southern Medical University, Guangzhou, Guangdong, China

[e]F.M. Kirby Research Center for Functional Brain Imaging, Kennedy Krieger Institute, Baltimore, MD, United States

Abstract

Amide proton transfer (APT) imaging is a novel MRI technique, in which the amide protons of endogenous proteins and peptides are irradiated to accomplish indirect detection using the bulk water signal. In this paper, the APT approach was added to a standard brain MRI protocol at 3T, and twelve patients with high-grade gliomas confirmed by histopathology were scanned. It is shown that all tumors, including one with minor gadolinium enhancement, showed heterogeneous hyperintensity on the APT images. The average APT signal intensities of the viable tumor cores were significantly higher than those of peritumoral edema and normal-appearing white matter ($P < 0.001$). The average APT signal intensities were significantly lower in the necrotic regions than in the viable tumor cores ($P = 0.004$). The APT signal intensities of the cystic cavities were similar to those of the viable tumor cores ($P > 0.2$). The initial results show that APT imaging at the protein and peptide level may enhance non-invasive identification of tissue heterogeneity in high-grade brain tumors.

Keywords

CEST; APT; magnetization transfer; brain tumor; protein; MRI

Introduction

High-grade gliomas in patients are invasive and histologically heterogeneous. These brain tumors typically consist of a solid tumor mass, often mixed with necrosis, and individual

*Corresponding authors: Fax: +86 20 8431 8988 or +1 410 614 1977. zhibowen@163.com (Zhibo Wen) or jzhou@mri.jhu.edu (Jinyuan Zhou).

Publisher's Disclaimer: This is a PDF file of an unedited manuscript that has been accepted for publication. As a service to our customers we are providing this early version of the manuscript. The manuscript will undergo copyediting, typesetting, and review of the resulting proof before it is published in its final citable form. Please note that during the production process errors may be discovered which could affect the content, and all legal disclaimers that apply to the journal pertain.

NIH-PA Author Manuscript
NIH-PA Author Manuscript
NIH-PA Author Manuscript

NIH-PA Author Manuscript

NIH-PA Author Manuscript

NIH-PA Author Manuscript

tumor cells infiltrating into edematous or even normal-appearing brain tissue (Burger et al., 1983; Kelly et al., 1987). Currently, these tumors are generally evaluated using gadolinium contrast-enhanced MRI, in combination with T2-weighted or fluid-attenuated inversion recovery (FLAIR) MRI, which are used to determine the extent of involvement, to guide treatments, and to assess a therapeutic response (Chang et al., 2009). However, existing MRI techniques are not sufficiently tissue-specific and suffer from several limitations. First, gadolinium enhancement on the post-contrast T1-weighted images reveals focal areas of tumor where the blood-brain barrier is disrupted, but it does not show large areas of infiltrating tumor (Kelly et al., 1987). Another limitation is that some high-grade gliomas demonstrate no gadolinium enhancement (Scott et al., 2002; Segall et al., 1990). In this case, it can be difficult to identify the most malignant portions of tumor prior to surgery or local therapies. Third, gadolinium enhancement is not always specific for tumor grade, as low-grade gliomas occasionally enhance (Knopp et al., 1999). Fourth, gadolinium enhancement occurs in any area of a blood-brain barrier disruption, such as treatment-related injury (Brandsma et al., 2008; Mullins et al., 2005), regardless of etiology. Finally, glioma patients require frequent MRI exams and gadolinium exposure has risk in patients with renal insufficiency (Broome, 2008). These imaging limitations have immediate clinical repercussions that may make diagnosis problematic and render local therapies ineffectual. In recent years, there has been much progress in tumor assessment using more advanced MRI approaches, including MR spectroscopy (Graves et al., 2001; Vigneron et al., 2001), diffusion imaging (Field and Alexander, 2004; Lu et al., 2004; Price et al., 2003; Sinha et al., 2002), perfusion imaging (Cha, 2004; Covarrubias et al., 2004), or a combination of these techniques (Catalaa et al., 2006; Law et al., 2003; Verma et al., 2008). Despite these, additional MR approaches, especially tissue-specific ones that use endogenous contrast agents, are much needed.

Amide proton transfer (APT) imaging is a new MRI technique that detects endogenous, low-concentration mobile proteins and peptides in tissue using a change in bulk water intensity due to saturation transfer of the amide protons in the peptide bonds (Zhou et al., 2003a; Zhou et al., 2003b). This technique, without the need for exogenous contrast agents, is based on the recently emerged chemical exchange saturation transfer (CEST) sensitivity enhancement approach (Aime et al., 2002; Ward et al., 2000; Zhang et al., 2001; Zhou and van Zijl, 2006). When applied to imaging of human brain tumors, the pilot clinical data suggested that APT might provide useful visual information about the presence and grade of brain tumors (Jones et al., 2006; Zhou et al., 2008), based on increased cellular protein and peptide levels in gliomas (Hobbs et al., 2003; Howe et al., 2003). The APT sequence is similar to the routinely used magnetization transfer contrast (MTC) sequences in the clinic (Wolff and Balaban, 1989), and it can be performed on any standard MRI platforms, including 7T (Mougin et al., 2010). The purpose of this study was to demonstrate that protein and peptide-based APT imaging could potentially enhance non-invasive identification of the heterogeneity of high-grade brain tumors, which is particularly important when gadolinium-enhanced T1-weighted MRI is not available.

Materials and Methods

Study Population

Twelve patients (nine male, three female; age range, 21-63 years; mean age, 42.9 years; see Table 1 for more information) with high-grade gliomas were included in this study. The studied neoplasms consisted of World Health Organization glioblastoma multiforme (grade IV astrocytoma) in four, grade III anaplastic astrocytoma in five, grade III anaplastic oligodendroglioma in one, the recurrence of grade III anaplastic astrocytoma in one, and the recurrence of grade III anaplastic oligodendroglioma in one. All diagnoses were confirmed

NIH-PA Author Manuscript

NIH-PA Author Manuscript

NIH-PA Author Manuscript

by histopathology. The study was approved by the local ethics committee, and written, informed consent was obtained from each patient.

MR Imaging

All patients were scanned on a Philips 3T MRI scanner (Achieva 3.0T; Philips Medical Systems, Best, The Netherlands) using a body coil for radiofrequency (RF) transmission and an eight-channel sensitivity-encoding coil for reception. The sequences performed for each patient included T1-weighted (repetition time = 2 sec; echo time = 20 msec), T2-weighted (repetition time = 3 sec; echo time = 80 msec), FLAIR (repetition time = 11 sec; inversion time = 2.2 sec; echo time = 125 msec), APT imaging, and gadolinium contrast-enhanced T1-weighted. For the routine MRI sequences, the field of view was 240 × 240 mm^2, the matrix was 512 × 512, and the slice thickness was 6 mm. After T1-weighted, T2-weighted, FLAIR, and APT scans were performed, 10 ml of gadopentetate dimeglumine (Magnevist; Bayer Schering, Guangzhou, China) was injected through the median cubital vein, and gadolinium-enhanced T1-weighted images were acquired.

It was shown previously (Zhou et al., 2008) that six-offset APT data acquisition (±3, ±3.5, ±4 ppm, 8 signal averages), together with a separately acquired z spectrum (33 offsets from 8 to -8 ppm with intervals of 0.5 ppm, one average), could provide B_0 inhomogeneity-corrected human brain APT images of sufficient signal-to-noise ratios within a clinically relevant time frame. In this study, a modified multi-offset, multi-acquisition APT imaging acquisition scheme (Table 2) was used, in which the APT image scan and z-spectrum scan were combined. To obtain the sufficient signal-to-noise ratios (~70; see the Discussion section) of the APT images, more acquisitions were placed at and around ±3.5 ppm. In addition, more offsets were used near 0 ppm for increasing the fitting accuracy of B0 maps; more offsets were used close to ±3.5 ppm for increasing the interpolation accuracy of APT data. Using the modified APT acquisition method, there was no need for the procedure to turn off the pre-scan between the two scans, which can affect the shim and frequency offset settings. The imaging parameters used were: RF saturation power = 3 μT; saturation time = 500 msec; repetition time = 3 sec; echo time = 11 msec; sensitivity-encoding factor = 2; matrix = 128×64; field of view = 240×240 mm^2; and slice thickness = 6 mm. One unsaturated image (no saturation pulses added) was acquired for control. The scanning time for this APT scan was about three minutes.

Image Analysis

All raw data were transferred to a Sun UltraSparc Station (Sun Microsystems, Mountain View, CA) for analysis, using programs written in interactive data language (IDL; Research Systems, Inc., Boulder, CO, USA). The definitions and nomenclature used in this study are equivalent to the previous papers (Jones et al., 2006; Zhou et al., 2008). Briefly, the magnetization transfer ratio (MTR) is defined as: $MTR = 1 - S_{sat}/S_0$, in which S_{sat} and S_0 are the signal intensities with and without selective RF irradiation, respectively. The calculated MTR asymmetry (MTR_{asym}) map at the offset of 3.5 ppm is called the APT image: $MTR_{asym}(3.5ppm) = MTR(+3.5ppm) - MTR(-3.5ppm) = S_{sat}(-3.5ppm)/S_0 - S_{sat}(+3.5ppm)/S_0$. In the data processing (Fig. 1), the raw data were first organized into the z-spectrum. Then, the z-spectrum was fitted on a pixel-by-pixel basis according to the procedure previously reported (Zhou et al., 2008), and the B0 inhomogeneity map was created. After this, the original z-spectrum was corrected for the B0 inhomogeneity effect through the interpolation and centering of the z-spectrum. Finally, the APT image was calculated and displayed in color using a window of -5% to 5%.

The quantitative image analysis was performed by two radiologists (ZW and XW, who had ~20 and 10 years of experience in brain tumor imaging, respectively). The results were

NIH-PA Author Manuscript

NIH-PA Author Manuscript

NIH-PA Author Manuscript

averaged for each tissue type for each subject. Five regions of interest were selected according to the signal abnormalities on the gadolinium-enhanced T1-weighted and other MR images, with the support of the histopathological findings. These regions of interest included the viable tumor core (with gadolinium enhancement or, if the gadolinium enhancement is not available, based on the FLAIR and T1-weighted MR images; see the Results section), necrosis (usually inside the lesion), cystic cavity (with the signal intensity similar to that of the cerebrospinal fluid on the T2-weighted images), immediate edema (adjacent to but distinct from the core of the tumor, usually within a 1-cm margin), and peripheral edema (outside the immediate-edema regions) (Oh et al., 2005). The ipsilateral and contralateral normal-appearing white matter was used for comparison.

Statistical Analysis

The average APT imaging intensities and corresponding 95% confidence intervals were calculated for each tissue type. The analysis of variance (ANOVA) post-hoc tests were used to determine whether the differences in APT intensities for various tissue types were significant. In addition, the average APT-MRI contrasts between tumor cores and peritumoral edema were calculated, and 95% confidence intervals were calculated for the mean contrasts. The level of significance was set at $P < 0.05$.

Results

Of 12 cases enrolled in this study, 11 tumors demonstrated clear gadolinium enhancement, and one had minor gadolinium enhancement; however, all tumors had markedly increased APT signals. Examples of APT imaging for patients who had pathologically-proven high-grade gliomas are shown in Figs 2-5. Figure 2 shows APT and standard anatomic MR images for a 21-year-old man (Patient 1) with an astrocytoma (grade III) in the right medial parietal lobe. Figure 3 demonstrates MRI data for a 45-year-old man (Patient 2) with recurrent astrocytoma (grade III) in the left parietal lobe. Figure 4 shows MR images for a 35-year-old man (Patient 3) with a glioblastoma multiforme in the left frontal lobe. Figure 5 demonstrates MR images of a 46-year-old woman (Patient 4) with a pathologically confirmed glioblastoma multiforme in the right frontal lobe. Figure 6 quantitatively compares the APT-MRI signal intensities from several regions of interest for all patients. Table 3 summarizes the statistical results of t-tests for the APT imaging intensities for various tissue types.

Tumor Core versus Peritumoral Edema

For 11 patients who had obvious gadolinium enhancement in this study, as shown in Figs 2-4, the gadolinium-enhancing tumor cores on the post-contrast T1-weighted images were all hyperintense on the APT images. Moreover, the area of maximal gadolinium enhancement for each case, which was associated with the most viable, actively growing aspect of the lesion (Burger et al., 1983;Kelly et al., 1987), corresponded well to the area of the highest intensity on the APT image. It seemed that the regions of increased APT extended outside the tumor core into peripheral brain zones (without gadolinium enhancement). When comparing the size of the lesions, the APT images were unique in that the APT-hyperintense areas were smaller than the abnormal areas on the T2-weighted or FLAIR images, but larger than or comparable to the lesions identified by the gadolinium-enhanced T1-weighted images. In addition, it is interesting that the gadolinium-enhancing cores of recurrent gliomas on the post-contrast T1-weighted images remained APT-hyperintense (Fig 3).

The case with minor gadolinium enhancement on the T1-weighted image also had elevated signal intensity on the APT image (Fig 5). In this case, the FLAIR image showed a large

NIH-PA Author Manuscript

NIH-PA Author Manuscript

NIH-PA Author Manuscript

heterogeneous mass with a zone of low signal intensity inside the lesion. On the pre-contrast T1-weighted image, the tumor was mostly hypointense, but mixed with an area of high signal intensity, which was consistent with the existence of hemorrhage. Although only the minor gadolinium enhancement was observed (part of the tumor, tumor rim), the noticeably high signal intensity appeared in most of the tumor on the APT image. This area of FLAIR hypointensity and T1-weighted hyperintensity on the pre-contrast T1-weighted image was a tumor mass, where high-density tumor cells were found by histopathology.

As shown in Fig 6, the average signal intensities of the tumor cores (3.8% ± 0.5%) on the APT images were significantly higher than those of the immediate edema (2.5% ± 0.6%, $P < 0.001$) and peripheral edema (2.2% ± 0.5%, $P < 0.001$). The average APT contrasts between the tumor cores and the immediate edema, and between the tumor cores and the peripheral edema were, respectively, 1.3% ± 0.6% and 1.6% ± 0.6%, with the 95% confidence intervals 0.9% to 1.6% and 1.2% to 2.0%, respectively. The average signal intensities were slightly higher in the immediate edema (2.5% ± 0.6%) than in the peripheral edema (2.2% ± 0.5%), but the difference was not statistically significant ($P > 0.2$).

Necrosis and Cystic Cavity

The viable tumor cores of malignant high-grade gliomas are often accompanied by necrosis and cyst formation. We found that these pathologically distinct lesions had markedly different characteristics on the APT images: low APT signal intensities in the necrotic areas (observed in nine of 12 patients; see Figs 2-4), and high APT signal intensities in the areas with cyst formation (observed in five of 12 patients; see Figs 4, 5). As shown in Fig 2, the gadolinium-enhanced T1-weighted image showed a multi-locular, ring-enhancing tumor mass in the right medial parietal lobe, surrounded by an area with hyperintense T2-weighted signal abnormality, nearly as bright as the cerebrospinal fluid, which was consistent with edema. The core of the tumor was obviously heterogeneous on the APT image, with APT hyperintensity in the gadolinium-enhancing ring and low APT signal intensities in the central necrotic area (without gadolinium enhancement).

On the other hand, as shown in Fig 5, there was a large area with cyst formation (with the high FLAIR signal) inside the tumor mass. This cystic area demonstrated the characteristic “fluid-fluid level” on the FLAIR image, which was filled with liquid-like, chronic hemorrhage, as confirmed during surgery. It is interesting that the cystic cavity with the lack of gadolinium enhancement on the post-contrast T1-weighted image showed hyperintensity on the APT image.

The average APT signal intensities were significantly lower in the necrotic regions (2.9% ± 0.6%) than in the viable tumor cores (3.8% ± 0.5%, $P = 0.004$). However, there was no significantly difference between the cystic components (4.0% ± 0.2%) and the viable tumor cores (3.8% ± 0.5%, $P > 0.2$) on the APT images.

Discussion

When using *in vivo* APT imaging, it is important to understand that although both APT and MTC (Wolff and Balaban, 1989) are magnetization transfer effects, they have different mechanisms and origins. Conventional MTC imaging is based on protons in immobile semi-solid macromolecules (such as structural proteins, membranes, and myelins), where saturation transfer occurs in multiple steps, both through dipolar coupling and chemical exchange. These solid-like protons have a very short T_2 and, therefore, resonate over a very large spectral width (±100 kHz) that does not allow selective RF irradiation of individual resonances. Thus, the z-spectrum appears to be almost symmetric around the water resonance. It has been demonstrated that MTC is useful for the characterization and

NIH-PA Author Manuscript

NIH-PA Author Manuscript

NIH-PA Author Manuscript

diagnosis of various brain diseases, such as glioma (Gong et al., 2004) and multiple sclerosis (Tozer et al., 2003). In contrast, APT imaging, with RF irradiation around 3.5 ppm from water to saturate the amide protons of mobile proteins and peptides in tissue, employs chemical exchange as a single transfer pathway to accomplish magnetization transfer. The frequency offset in APT experiments is limited to a small range around the water resonance, and two proton pools can be distinguished from each other on the NMR time scale. This leads to a clear asymmetry in the z-spectrum with respect to the water resonance, such that the APT effect can be separated from MTC and direct saturation by determining the asymmetry in MTR at ±3.5 ppm.

The viable, actively growing tumor cores in high-grade gliomas demonstrate the high signal intensities on the APT images. Although some tumors do not enhance on the gadolinium-enhanced T1-weighted images, the high signal intensities still exist for the tumors on the APT images. The APT signal intensities of these tumor cores are significantly higher than those of the immediate edema, peripheral edema, and normal-appearing white matters. The clear APT hyperintensity is thus a typical feature of the tumor, suggesting a higher mobile protein and peptide concentration, as measured previously by MRI-guided proteomics (Hobbs et al., 2003) and *in vivo* MR spectroscopy (Howe et al., 2003). Recently, in an initial MRI-proteomics correlation experiment, Hobbs et al. (Hobbs et al., 2003) found that protein expression profiles correlated with gadolinium enhancement in human glioblastoma multiforme. More protein species and higher protein expression levels were seen in gadolinium-enhancing than in non-enhancing regions. In addition, using *in vivo* proton MRS, Howe et al. (Howe et al., 2003) showed that the MRS-detectable mobile macromolecular proton concentration was higher in human brain tumors than in normal white matter, and increased with tumor grade. Here, it is important to notice that the aliphatic signals studied by Howe et al. (Howe et al., 2003) are related to the 8.3 ppm amide resonance through the intramolecular nuclear Overhauser effects between these proton groups, as shown in our recent water exchange experiments (Zhou et al., 2003b).

The edema, which usually encircles the tumor core, is an area of T2-weighted or FLAIR hyperintensity, nearly as bright as the cerebrospinal fluid, due to higher water content. The edematous area surrounding a malignant glioma is often infiltrated by isolated tumor cells, and it may have a higher T2-weighted (or FLAIR) signal abnormality than the tumor core. However, the boundary between the edema regions and tumor cores is generally not clear. As shown in Figs 2-5, both the solid tumor masses and the peritumoral edema are hyperintense on the T2-weighted images or FLAIR images; thus, they are indistinguishable with conventional MR images. However, the edematous areas clearly have the low APT signals for all patients. Therefore, these two components may be simply distinguished with APT imaging. Furthermore, the APT signal intensity of immediate edema is a little higher than the peripheral-edema regions, even though the difference was not statistically significant. The tendency that the regions of increased APT extend outside the tumor core (usually signified by gadolinium enhancement) into the peripheral brain zones may represent tumor infiltration, but more evaluations are needed.

The masses of solid tumors are histologically heterogeneous. Our preliminary results in this study show that APT imaging, when added into the conventional MR imaging, may help identify the different components of high-grade gliomas. As shown in Figs 2-4, the non-enhancing necrotic regions inside the solid tumor cores seem isointense on the APT images. The average APT signal intensity in the necrotic regions, which is similar to those of immediate edema and peripheral edema, is significantly lower than that of the enhancing viable tumor cores. Unlike the necrotic regions, the cystic areas of the tumor cores are hyperintense on the APT images, as shown in Figs 4, 5. The average signal intensity of the cystic cavities, similar to that of the viable tumor cores, is significantly higher than those of

NIH-PA Author Manuscript

NIH-PA Author Manuscript

NIH-PA Author Manuscript

the necrosis, immediate edema, and peripheral edema. It is possible that there exists a large amount of mobile proteins and peptides in the liquid-like cystic cavities, thus resulting in the increase in APT detectability.

There were two cases (Patients 2, 8) of recurrent high-grade gliomas in this study. The results show that the gadolinium-enhancing cores of recurrent gliomas on the post-contrast T1-weighted images still show hyperintensity on the APT images (Fig 3), with the APT signal intensities similar to those of the newly diagnosed tumors. The standard of care for patients with brain tumors is maximal surgery and concurrent chemotherapy and radiation therapy. Although this regimen improves survival, the associated risk for brain injury also increases. The treatment-induced injury can exactly mimic tumor recurrence, both clinically and radiographically (Brandsma et al., 2008;Mullins et al., 2005), including the signal abnormality on T2-weighted or FLAIR images, gadolinium enhancement on post-contrast T1-weighted images, and mass effect. This has complicated daily patient care and is a critical barrier to investigating the efficacy of new therapies for brain tumors. The APT signals may be used as an imaging biomarker for assessing disease progression (APT hyperintense) and treatment-related injury, such as radiation necrosis (APT isointense or even hypointense).

There are some limitations for the APT approach. (i) In addition to the mobile protein and peptide concentration, some other physico-chemical (tissue water content, pH, and temperature) and technical (T1 of water) may affect the APT signal. Fortunately, as discussed in our previous papers (Zhou et al., 2003a; Zhou et al., 2003b; Zhou et al., 2008), increased APT intensities in the tumor with respect to the non-tumorous brain tissue can be attributed mainly to increased protein and peptide content (Hobbs et al., 2003; Howe et al., 2003). (ii) The APT signal in the brain at 3T is relatively small, about 2-4% of the bulk water intensity. The APT image contrast between the tumor and the non-tumorous parenchyma is also small, which is ~1.5-2%. To obtain the reliable results, the calculated APT images should have a signal-to-noise ratio of ~70 or better, corresponding to a signal-to-noise ratio of ~100 or better for the acquired saturated images at ±3.5ppm. When designing an imaging protocol, more acquisitions should thus be placed at and around ±3.5 ppm. (iii) There are often some artifacts near the surface of brain and ventricles on the APT images. These artifacts could be caused by head motion. To avoid the misinterpretation, combining the APT images with high-resolution standard MRI is recommended. (iv) The spatial resolution of APT images is much lower than that of other conventional MR images due to the small APT effect. We except that this can be improved in the near future with a high performance multiple-channel phased-array RF coil or 7T, where the signal-to-noise ratios would be increased significantly (Mougin et al., 2010).

In conclusion, early results as presented in this paper suggest that APT imaging may be able to identify the most active parts of the tumors, without the need for an exogenous contrast agent. The addition of APT imaging to the standard MRI protocol may thus help distinguish the heterogeneity of malignant brain tumors in a non-invasive manner. Once the point-to-point radiopathologic correlation is further performed in the future, these unique capabilities of APT imaging may be very important for assisting with diagnosis and treatment planning for patients with brain tumors, including non-enhancing high-grade tumors, by providing more accurate targets for surgery and radiation therapy.

Acknowledgments

The authors thank Ms. Mary McAllister for editorial assistance. This work was supported in part by grants from NIH (EB009112, EB009731, and RR015241), and the Dana Foundation.

NIH-PA Author Manuscript

NIH-PA Author Manuscript

NIH-PA Author Manuscript

References

Aime S, Barge A, Delli Castelli D, Fedeli F, Mortillaro A, Nielsen FU, Terreno E. Paramagnetic Lanthanide(III) complexes as pH-sensitive chemical exchange saturation transfer (CEST) contrast agents for MRI applications. Magn Reson Med 2002;47:639–648. [PubMed: 11948724]

Brandsma D, Stalpers L, Taal W, Sminia P, van den Bent MJ. Clinical features, mechanisms, and management of pseudoprogression in malignant gliomas. Lancet Oncol 2008;9:453–461. [PubMed: 18452856]

Broome DR. Nephrogenic systemic fibrosis associated with gadolinium based contrast agents: A summary of the medical literature reporting. Eur J Radiol 2008;66:230–234. [PubMed: 18372138]

Burger PC, Dubois PJ, Schold SCJ, Smith KRJ, Odom GL, Crafts DC, Giangaspero F. Computerized tomographic and pathologic studies of the untreated, quiescent, and recurrent glioblastoma multiforme. J Neurosurg 1983;58:159–169. [PubMed: 6294260]

Catalaa I, Henry R, Dillon WP, Graves EE, McKnight TR, Lu Y, Vigneron DB, Nelson SJ. Perfusion, diffusion and spectroscopy values in newly diagnosed cerebral gliomas. NMR Biomed 2006;19:463–475. [PubMed: 16763973]

Cha S. Perfusion MR imaging of brain tumors. Top Magn Reson Imag 2004;15:279–289.

Chang SM, Nelson S, Vandenberg S, Cha S, Prados M, Butowski N, McDermott M, Parsa AT, Aghi M, Clarke J, Berger M. Integration of preoperative anatomic and metabolic physiologic imaging of newly diagnosed glioma. J Neuro-Oncol 2009;92:401–415.

Covarrubias DJ, Rosen BR, Lev MH. Dynamic magnetic resonance perfusion imaging of brain tumors. Oncologist 2004;9:528–537. [PubMed: 15477637]

Field AS, Alexander AL. Diffusion tensor imaging in cerebral tumor diagnosis and therapy. Top Magn Reson Imag 2004;15:315–324.

Gong QY, Eldridge PR, Brodbelt AR, Garcia-Finana M, Zaman A, Jones B, Roberts N. Quantification of tumor response to radiotherapy. British J Radiol 2004;77:405–413.

Graves EE, Nelson SJ, Vigneron DB, Verhey L, McDermott M, Larson D, Chang S, Prados MD, Dillon WP. Serial proton MR spectroscopic imaging of recurrent malignant gliomas after gamma knife radiosurgery. AJNR Am J Neuroradiol 2001;22:613–624. [PubMed: 11290467]

Hobbs SK, Shi G, Homer R, Harsh G, Altlas SW, Bednarski MD. Magnetic resonance imaging-guided proteomics of human glioblastoma multiforme. J Magn Reson Imag 2003;18:530–536.

Howe FA, Barton SJ, Cudlip SA, Stubbs M, Saunders DE, Murphy M, Wilkins P, Opstad KS, Doyle VL, McLean MA, Bell BA, Griffiths JR. Metabolic profiles of human brain tumors using quantitative in vivo ^{1}H magnetic resonance spectroscopy. Magn Reson Med 2003;49:223–232. [PubMed: 12541241]

Jones CK, Schlosser MJ, van Zijl PC, Pomper MG, Golay X, Zhou J. Amide proton transfer imaging of human brain tumors at 3T. Magn Reson Med 2006;56:585–592. [PubMed: 16892186]

Kelly PJ, Daumas-Duport C, Kispert DB, Kall BA, Scheithauer BW, Illig JJ. Imaging-based stereotaxic serial biopsies in untreated intracranial glial neoplasms. J Neurosurg 1987;66:865–874. [PubMed: 3033172]

Knopp EA, Cha S, Johnson G, Mazumdar A, Golfinos JG, Zagzag D, Miller DC, Kelly PJ, Kricheff II. Glial neoplasms: dynamic contrast-enhanced T2*-weighted MR imaging. Radiology 1999;211:791–798. [PubMed: 10352608]

Law M, Yang S, Wang H, Babb JS, Johnson G, Cha S, Knopp EA, Zagzag D. Glioma grading: sensitivity, specificity, and predictive values of perfusion MR imaging and proton MR spectroscopic imaging compared with conventional MR imaging. AJNR Am J Neuroradiol 2003;24:1989–1998. [PubMed: 14625221]

Lu S, Ahn D, Johnson G, Law M, Zagzag D, Grossman RI. Diffusion-tensor MR imaging of intracranial neoplasia and associated peritumoral edema: Introduction of the tumor infiltration index. Radiology 2004;232:221–228. [PubMed: 15220505]

Mougin OE, Coxon RC, Pitiot A, Gowland PA. Magnetization transfer phenomenon in the human brain at 7T. NeuroImage 2010;49:272–281. [PubMed: 19683581]

NIH-PA Author Manuscript

NIH-PA Author Manuscript

NIH-PA Author Manuscript

Mullins ME, Barest GD, Schaefer PW, Hochberg FH, Gonzalez RG, Lev MH. Radiation necrosis versus glioma recurrence: conventional MR imaging clues to diagnosis. AJNR Am J Neuroradiol 2005;26:1967–1972. [PubMed: 16155144]

Oh J, Cha SM, Aiken AH, Han ET, Crane JC, Stainsby JA, Wright GA, Dillon WP, Nelson SJ. Quantitative apparent diffusion coefficients and T2 relaxation times in characterizing contrast enhancing brain tumors and regions of peritumoral edema. J Magn Reson Imag 2005;21:701–708.

Price SJ, Burnet NG, Donovan T, Green HAL, Pena A, Antoun NM, Pickard JD, Carpenter TA, Gillard JH. Diffusion tensor Imaging of brain tumours at 3T: A potential tool for assessing white matter tract invasion? Clin Radiology 2003;58:455–462.

Scott JN, Brasher PM, Sevick RJ, Rewcastle NB, Forsyth PA. How often are nonenhancing supratentorial gliomas malignant? A population study. Neurology 2002;59:947–949. [PubMed: 12297589]

Segall, HD.; Destian, S.; Nelson, MD. CT and MR imaging in malignant gliomas. In: Apuzzo, MLJ., editor. Malignant cerebral glioma. American Association of Neurological Surgeons; Park Ridge, IL: 1990. p. 63-78.

Sinha S, Bastin ME, Whittle IR, Wardlaw JM. Diffusion tensor MR imaging of high-grade cerebral gliomas. AJNR 2002;23:520–527. [PubMed: 11950638]

Tozer D, Ramani A, Barker GJ, Davies GR, Miller DH, Tofts PS. Quantitative magnetization transfer mapping of bound protons in multiple sclerosis. Magn Reson Med 2003;50:83–91. [PubMed: 12815682]

Verma R, Zacharaki EI, Ou Y, Cai H, Chawla S, Lee SK, Melhem ER, Wolf R, Davatzikos C. Multiparametric tissue characterization of brain neoplasms and their recurrence using pattern classification of MR images. Acad Radiol 2008;15:966–977. [PubMed: 18620117]

Vigneron D, Bollen A, McDermott M, Wald L, Day M, Moyher-Noworolski S, Henry R, Chang S, Berger M, Dillon W, Nelson S. Three-dimensional magnetic resonance spectroscopic imaging of histologically confirmed brain tumors. Magn Reson Imag 2001;19:89–101.

Ward KM, Aletras AH, Balaban RS. A new class of contrast agents for MRI based on proton chemical exchange dependent saturation transfer (CEST). J Magn Reson 2000;143:79–87. [PubMed: 10698648]

Wolff SD, Balaban RS. Magnetization transfer contrast (MTC) and tissue water proton relaxation in vivo. Magn Reson Med 1989;10:135–144. [PubMed: 2547135]

Zhang S, Winter P, Wu K, Sherry AD. A novel europium(III)-based MRI contrast agent. J Am Chem Soc 2001;123:1517–1578. [PubMed: 11456734]

Zhou J, Blakeley JO, Hua J, Kim M, Laterra J, Pomper MG, van Zijl PCM. Practical data acquisition method for human brain tumor amide proton transfer (APT) imaging. Magn Reson Med 2008;60:842–849. [PubMed: 18816868]

Zhou J, Lal B, Wilson DA, Laterra J, van Zijl PCM. Amide proton transfer (APT) contrast for imaging of brain tumors. Magn Reson Med 2003a;50:1120–1126. [PubMed: 14648559]

Zhou J, Payen J, Wilson DA, Traystman RJ, van Zijl PCM. Using the amide proton signals of intracellular proteins and peptides to detect pH effects in MRI. Nature Med 2003b;9:1085–1090. [PubMed: 12872167]

Zhou J, van Zijl PC. Chemical exchange saturation transfer imaging and spectroscopy. Progr NMR Spectr 2006;48:109–136.

NIH-PA Author Manuscript

NIH-PA Author Manuscript

NIH-PA Author Manuscript

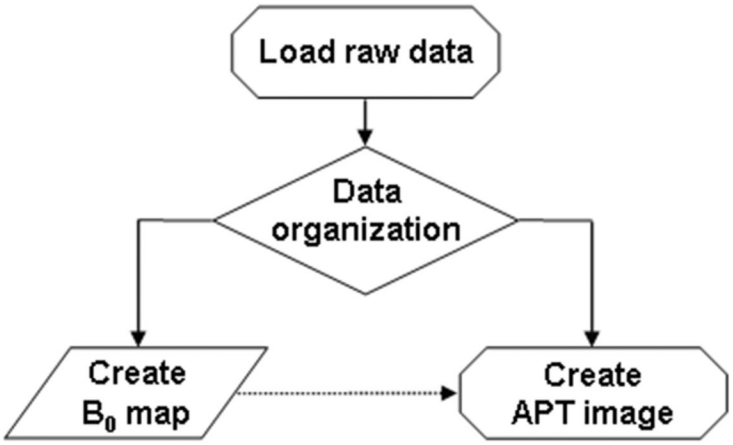

Fig. 1.

Flow chart of APT imaging data processing. After raw data are loaded and organized, the procedure is divided into the generation of a B0 map and the correction of APT data using the B0 map.

NIH-PA Author Manuscript
NIH-PA Author Manuscript
NIH-PA Author Manuscript

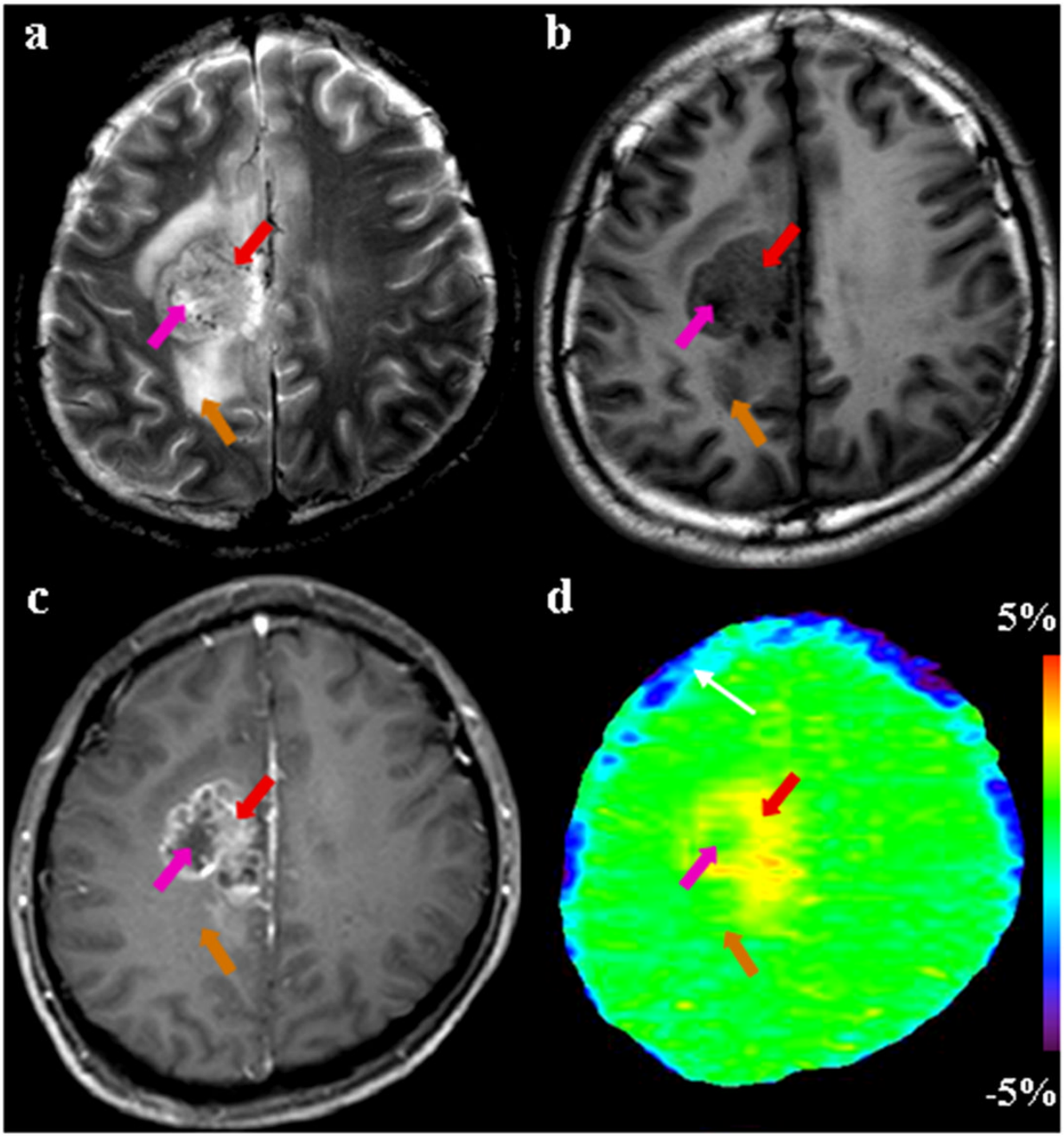

Fig. 2.

MR images for a patient with astrocytoma (grade III). (a) T2-weighted image shows a heterogeneously hyperintense focus in the right medial parietal lobe. (b) T1-weighted image shows that the entire tumor is hypointense. (c) Gadolinium-enhanced T1-weighted image demonstrates the typical imaging characteristics of a high-grade glioma: an enhancing tumor core (red arrow) with a non-enhancing necrotic area (pink arrow). (d) APT image shows that the tumor core (red arrow) is hyperintense, while the necrotic region (pink arrow) and edema area (orange arrow) have low APT signals. The blue strip (white arrow) adjacent to the surface of brain on the APT image may be the artifact caused by head motion.

NIH-PA Author Manuscript
NIH-PA Author Manuscript
NIH-PA Author Manuscript

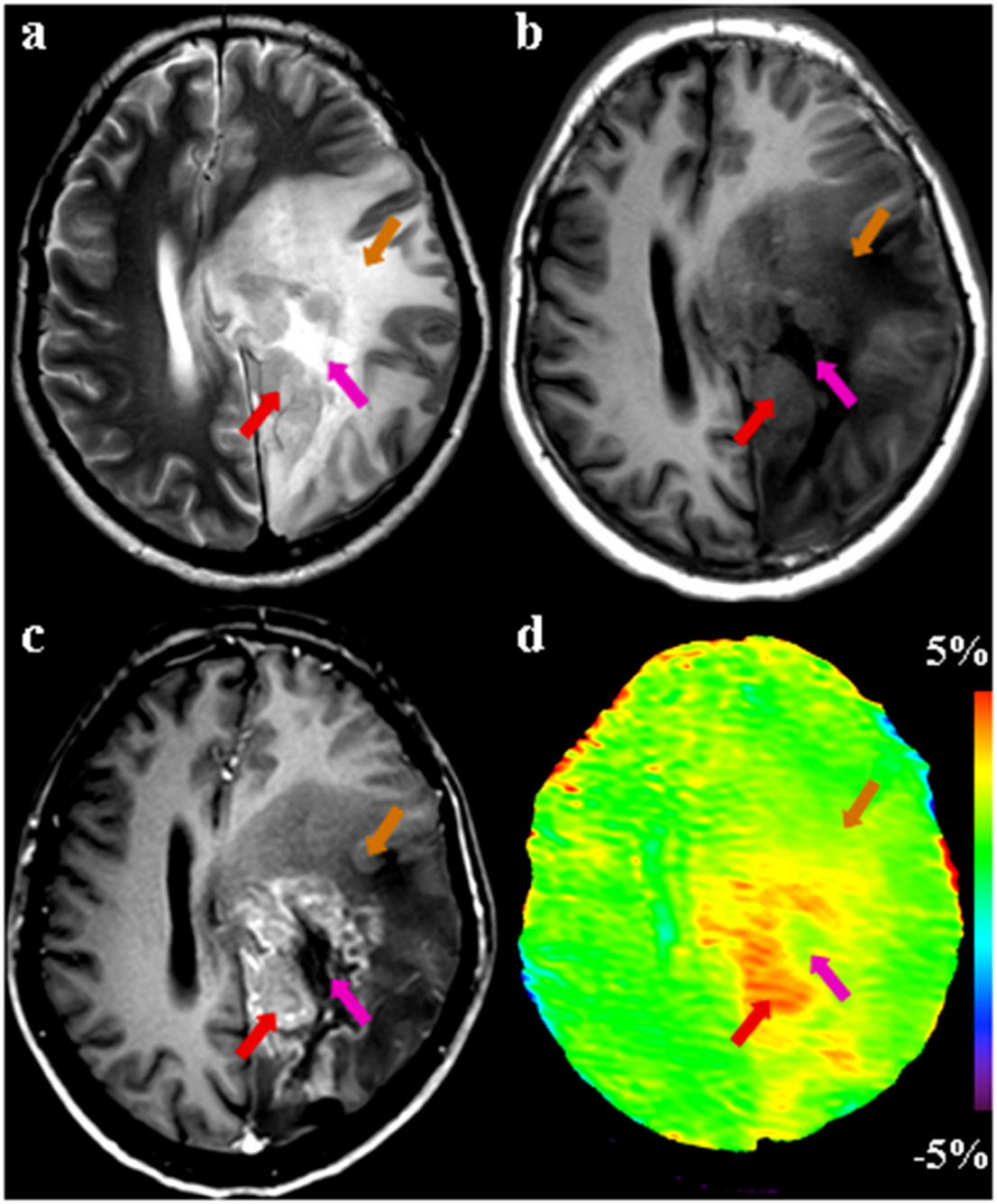

Fig. 3.

MR images from a patient with recurrent astrocytoma (grade III), acquired four months after treatment. (a) T2-weighted image shows the recurrence of glioma with heterogeneous hyperintensity in the left parietal lobe. (b) T1-weighted image shows a heterogeneously hypointense lesion. The exact location of the tumor core is not clear. (c) Post-contrast T1-weighted image reveals a gadolinium-enhancing tumor core (red arrow) and a necrotic area (pink arrow). The recurrent tumor is associated with the surrounding edema and mass effect. (d) APT image shows that there is a clear increase in APT signal intensity in the tumor core, identified by the gadolinium-enhanced T1-weighted image. The regions of necrosis (pink arrow) and edema (orange arrow) are almost isointense on APT.

NIH-PA Author Manuscript

NIH-PA Author Manuscript

NIH-PA Author Manuscript

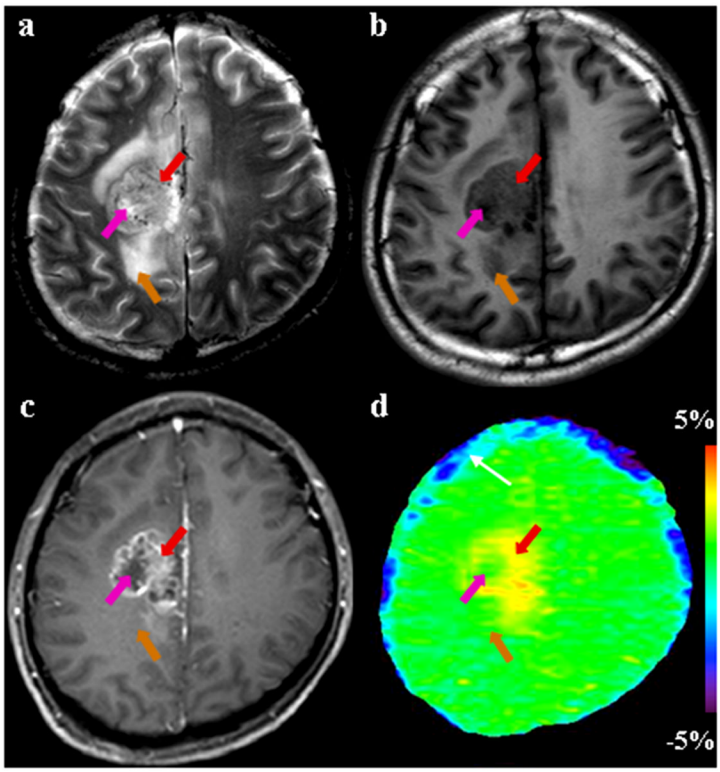

Fig. 4.

MR images for a patient with glioblastoma multiforme. (a) T2-weighted image demonstrates a large tumor of abnormal signals in the left frontal lobe. The area with cyst formation (black arrow) is clearly visible. (b) T1-weighted image shows that the entire tumor is hypointense. (c) Gadolinium-enhanced T1-weighted image demonstrates an enhancing tumor core (red arrow) with non-enhancing necrotic areas. (d) APT image shows that both the gadolinium-enhancing tumor core (red arrow) and the cystic cavity (black arrow) have high APT signal intensities, while the necrotic regions (pink arrow) and edema areas (orange arrow) have low APT signal intensities.

NIH-PA Author Manuscript

NIH-PA Author Manuscript

NIH-PA Author Manuscript

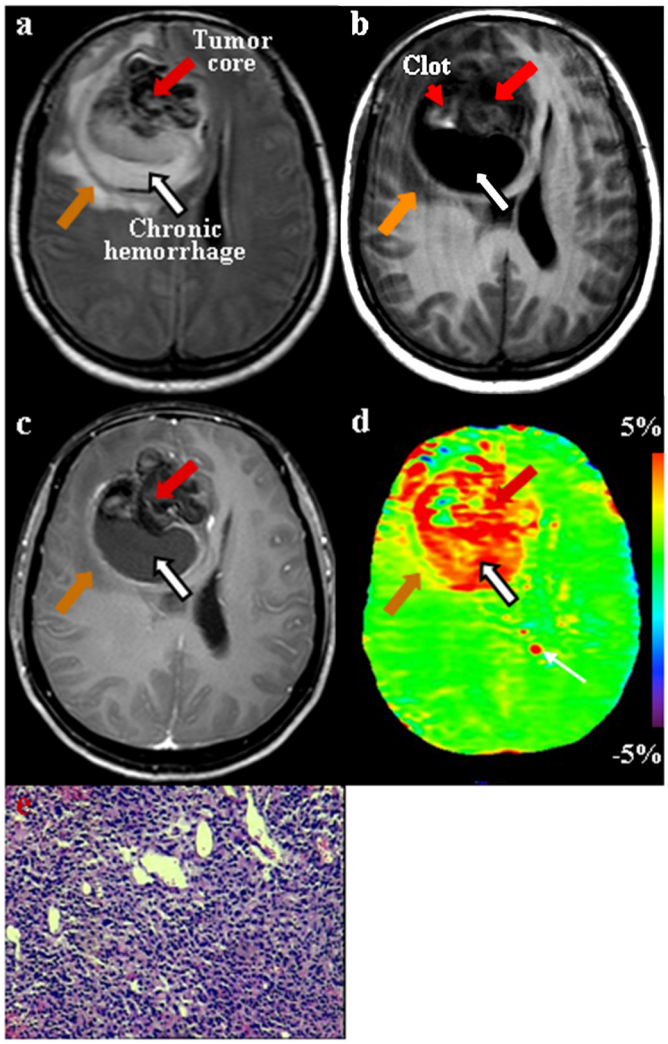

Fig. 5.

MR images for a patient with glioblastoma multiforme. (a) FLAIR image shows a large tumor of heterogeneous signal intensities in the right frontal lobe. The hypointense region may represent hemorrhage. (b) T1-weighted image demonstrates that the entire tumor is mostly hypointense, with a small region of high signal intensities (red arrowhead) that is the characteristic of hemorrhage. (c) Gadolinium-enhanced T1-weighted image shows a slightly enhancing tumor core (red arrow) with a non-enhancing cystic cavity (black arrow) filled with liquid-like, chronic hemorrhage. (d) APT image shows that both the tumor core (red arrow) and the cystic cavity (black arrow) generally have high APT signals, while the clot (red arrowhead) has a low APT signal. The red spot (white arrow) near the ventricle on the APT image was an artifact. (e) H&E-stained brain section (×50) confirms the existence of high-density multi-form tumor cells in the tumor core (red arrow).

NIH-PA Author Manuscript

NIH-PA Author Manuscript

NIH-PA Author Manuscript

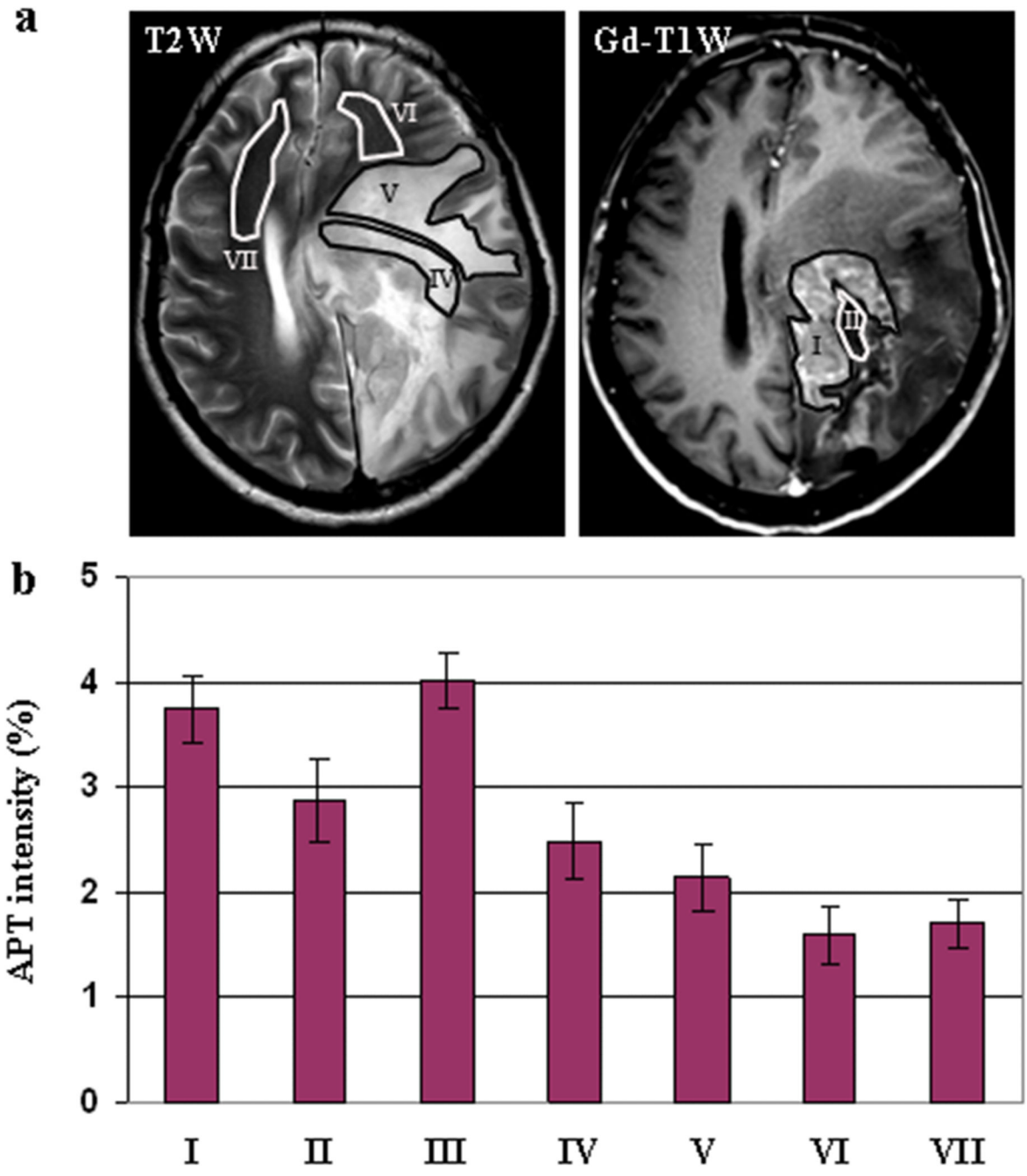

Fig. 6.

Quantitative analysis of the APT images from all patients studied in this work. (a) Examples of the definition of the regions of interest. (b) Average APT intensities and corresponding 95% confidence intervals plotted as a function of tissue type. (I) viable tumor core; (II) necrosis; (III) cystic component; (IV) immediate edema; (V) peripheral edema; (VI) ipsilateral normal-appearing white matter; (VII) contralateral normal-appearing white matter. The APT intensity is the percentage of the bulk water signal.

NIH-PA Author Manuscript
NIH-PA Author Manuscript
NIH-PA Author Manuscript

Table 1

Patient characteristics and pathology

No.	Age	Sex	Lesion location	Clinical presentation	Pathology
1	21	M	Right parietal	Headache	Astrocytoma, Grade III
2	45	M	Left parietal	Seizure	Recurrence of astrocytoma, Grade III
3	35	M	Left frontal	Seizure	Glioblastoma multiforme
4	46	F	Right frontal	Headache	Glioblastoma multiforme
5	61	M	Left frontal	Weakness of right limbs	Glioblastoma multiforme
6	63	M	Right temporal	Weakness of left limbs	Astrocytoma, Grade III
7	32	F	Left basal ganglia	Weakness of right limbs	Glioblastoma multiforme
8	34	M	Left temporal	Seizure	Recurrence of anaplastic oligodendroglioma, Grade III
9	47	F	Left occipital	Weakness of right limbs	Astrocytoma, Grade III
10	38	M	Left temporal	Weakness of right limbs	Astrocytoma, Grade III
11	43	M	Right parietal-occipital	Headache	Anaplastic oligodendroglioma, Grade III
12	50	M	Left parietal-occipital	Seizure and weakness of left limbs	Astrocytoma, Grade III

NIH-PA Author Manuscript

NIH-PA Author Manuscript

NIH-PA Author Manuscript

Table 2

APT imaging acquisition scheme

Offset (ppm)	NA	Offset (ppm)	NA
0	1	±3	2
±0.25	1	±3.25	4
±0.5	1	±3.5	8
±0.75	1	±3.75	4
±1	1	±4	2
±1.5	1	±4.5	1
±2	1	±5	1
±2.5	1	±6	1

One image without RF irradiation was acquired for signal normalization. NA stands for the number of acquisitions.

NIH-PA Author Manuscript
NIH-PA Author Manuscript
NIH-PA Author Manuscript

Table 3

P-values of ANOVA post-hoc tests for the APT imaging intensities

	Necrosis	Cystic	IE	PE	INAWM	CNAWM
Viable	0.004	> 0.2	< 0.001	< 0.001	< 0.001	< 0.001
Necrosis		0.003	> 0.2	0.03	< 0.001	< 0.001
Cystic			< 0.001	< 0.001	< 0.001	< 0.001
IE				> 0.2	0.001	0.007
PE					0.1	> 0.2
INAWM						> 0.2

Viable tumor core (viable), necrosis, cystic cavity (cystic), immediate edema (IE), peripheral edema (PE), and ipsilateral and contralateral normal-appearing white matter (INAWM, CNAWM).